electronics

MDPI

Article

High Sound-Contrast Inverse Scattering by MR-MF-DBIM Scheme

Luong Thi Theu [1], Tran Quang-Huy [2], Tran Duc-Nghia [3], Vijender Kumar Solanki [4], Tran Duc-Tan [5] and João Manuel R. S. Tavares [6,*]

[1] Institute of Applied Technology, Thu Dau Mot University, Binh Duong 820000, Vietnam
[2] Faculty of Physics, Hanoi Pedagogical University 2, Hanoi 100000, Vietnam
[3] Institute of Information Technology, Vietnam Academy of Science and Technology, Hanoi 100000, Vietnam
[4] CMR Institute of Technology, Hyderabad, Telangana 501401, India
[5] Faculty of Electrical and Electronic Engineering, Phenikaa University, Hanoi 12116, Vietnam
[6] Instituto de Ciência e Inovação em Engenharia Mecânica e Engenharia Industrial, Departamento de Engenharia Mecânica, Faculdade de Engenharia, Universidade do Porto, 4200-465 Porto, Portugal
* Correspondence: tavares@fe.up.pt

Abstract: In ultrasound tomography, cross-sectional images represent the spatial distribution of the physical parameters of a target of interest, which can be obtained based on scattered ultrasound measurements. These measurements can be obtained from dense datasets collected at different transmitter and receiver locations, and using multiple frequencies. The Born approximation method, which provides a simple linear relationship between the objective function and the scattering field, has been adopted to resolve the inverse scattering problem. The distorted Born iterative method (DBIM), which utilizes the first-order Born approximation, is a productive diffraction tomography scheme. In this article, the range of interpolation applications is extended at the multilayer level, taking into account the advantages of integrating this multilayer level with multiple frequencies for the DBIM. Specifically, we consider: (a) a multi-resolution technique, i.e., a multi-step interpolation for the DBIM: MR-DBIM, with the advantage that the normalized absolute error is reduced by 18.67% and 37.21% in comparison with one-step interpolation DBIM and typical DBIM, respectively; (b) the integration of multi-resolution and multi-frequency techniques with the DBIM: MR-MF-DBIM, which is applied to image targets with high sound contrast in a strongly scattering medium. Relative to MR-DBIM, this integration offers a 44.01% reduction in the normalized absolute error.

Keywords: ultrasound tomography; distorted Born iterative method; multi-resolution; multi-frequency

check for updates

Citation: Theu, L.T.; Quang-Huy, T.; Duc-Nghia, T.; Solanki, V.K.; Duc-Tan, T.; Tavares, J.M.R.S. High Sound-Contrast Inverse Scattering by MR-MF-DBIM Scheme. *Electronics* **2022**, *11*, 3203. https://doi.org/10.3390/electronics11193203

Academic Editors: Peter Sarcevic, Sašo Tomažič, Akos Odry, Sara Stančin and Gábor Kertész

Received: 30 August 2022
Accepted: 27 September 2022
Published: 6 October 2022

Publisher's Note: MDPI stays neutral with regard to jurisdictional claims in published maps and institutional affiliations.

Copyright: © 2022 by the authors. Licensee MDPI, Basel, Switzerland. This article is an open access article distributed under the terms and conditions of the Creative Commons Attribution (CC BY) license (https://creativecommons.org/licenses/by/4.0/).

1. Introduction

Acoustical imaging techniques have been widely used since the invention of sonar technology. One of the most popular ultrasound imaging techniques based on the sonar principle is B-mode imaging [1], which is mainly used in non-destructive evaluation and medical imaging. The B-mode image qualitatively represents the change in the acoustic impedance function, which allows the viewer to distinguish the different media. The spatial images can be obtained by using a transducer array [2] and a detector element probe with high convergence properties [3]. Although the quality of the acquired image may deteriorate due to amplitude and phase variations [4], B-mode imaging is simple and reliable. However, due to the naturally qualitative properties of the B-mode images, medical diagnosis using this imaging technique is often subjective, because it is strongly dependent on the expertise of the physicians.

Nevertheless, the acquired acoustic data contains much more information than is usually acquired using the B-mode scheme. Therefore, researchers have given their attention to the backscatter theory of ultrasonic waves. One of the limitations of backscatter techniques is the lack of robust and efficient computational techniques. The first algorithm, which was developed in the early 1970s, was based on the projection theory used in radiography and

nuclear tomography imaging. This algorithm reconstructs the sound speed map [5] and attenuation [6]. However, unlike other tomography methods, linear propagation is not a realistic model of sound wave propagation in biological media. Although the refractive correction technique has been developed to extend the validity of the linear propagation algorithm [7], these methods face limitations in terms of spatial resolution and abnormal components associated with diffraction. Thus, these techniques have only achieved limited success. Therefore, ultrasound tomography was developed to overcome some of the limitations of the straight-ray method.

The ultrasound tomography technique is based on the scattering effect. Whenever an incident ultrasound wave meets a non-uniform domain, scattered data occur in every direction around this domain. A set of scattering measurements is performed by inversing the wave equation. The main problem in ultrasound tomography is the estimation of the distribution of acoustic parameters in the scattering environment, such as sound contrast, sound attenuation, and density. Therefore, ultrasound tomography can present the quantitative information of the examined target. At present, there are few ultrasound computed tomography (UCT) systems used in clinical diagnostics. Two of these systems are computerized ultrasound risk evaluation (CURE) [8,9] and high-resolution ultrasonic transmission tomography (HUTT) [10] systems, which can reconstruct the images based on the parameters of sound contrast and attenuation. However, these systems' spatial resolution and accuracy are limited because their algorithms have ignored the effects of diffraction. Another ultrasound tomography system is the transcranial magnetic stimulation (TMS) system [11], which provides a more detailed description of the object of interest. Besides the sound impedance parameter, several other parameters must also be considered for imaging. B-mode imaging provides purely qualitative information about the object of interest, whereas backscatter gives quantitative information regarding the object's mechanical properties.

However, acoustic inverse scattering also has some limitations. As a result, ultrasound tomography devices have not achieved the same success as other techniques, such as X-ray and nuclear magnetic resonance imaging [12]. Firstly, inverse scattering techniques meet with convergence problems while reconstructing an object with high contrast. Thus, their application has been limited to breast tissue [13–15]. In order to extend the range of applications, further research projects have been undertaken concerning bone imaging [16]. Secondly, scattered data must be acquired from many different angles from 0 to 360° in order to achieve the best image quality.

Ultrasound tomography is based on first-order approximations to the wave equation using the Born approximation method [17] or Rytov modeling [18]. The Born iterative method (BIM) and the distorted Born iterative method (DBIM) are two of the leading scattering imaging methods [19,20], although these approaches still have complications because they must resolve a large number of iterations and solve the inverse problem. Mainly concerning breast imaging, it was demonstrated in [21] that the DBIM-based iterative algorithm is efficient and accurate. Using 16 probes, the authors detected a simulated anomaly. Then, in [22], experiments were performed by adding two more rings of 16 probes in order to improve the resolution of the reconstructed images. The model's performance was then compared using the root-mean-square error (RMSE) and Pearson's correlation coefficient.

The multi-resolution (MR) technique, mainly the interpolation technique, was studied and applied to the DBIM in [23,24]. Initially, the objective function is recovered for the matrix of $N_1 \times N_1$ size, and then, an interpolation technique is used to obtain a larger ($N_2 \times N_2$) matrix. The quality of the recovered images by this scheme is better than that of the DBIM, and the computation time is also significantly reduced. The multi-frequency (MF) technique has been studied and applied to the DBIM in [25–37]. This approach is applied as follows: in the first step, the lower frequency acquired data are used to ensure fast convergence, and in the second step, the higher frequency acquired data are used to ensure the high resolution of the reconstructed image.

This work suggests a method to enhance the reconstruction quality of ultrasound tomography by using multi-resolution and multi-frequency methods. Firstly, a multi-resolution technique is considered for the DBIM: MR-DBIM. Secondly, the integration of multi-resolution and multi-frequency techniques is studied for the DBIM: MR-MF-DBIM, with the aim of imaging targets of high sound contrast in the strongly scattering domain. As a result, the normalized error and total time for reconstruction are significantly reduced.

2. Materials and Methods

Figure 1 shows the studied imaging configuration, which has a circular shape, and the probes, i.e., the transmitters/receivers, which are evenly arranged on the measurement system. The 2D zero-order Bessel function [38] is used as the incident beam emitted by the transmitter, and is expressed as:

$$\overline{p}^{inc} = J_0(k_0|r - r_k|) \tag{1}$$

where J_0 is the Bessel function of zero-order, k_0 is the wave number of the background medium, and $|r - r_k|$ is the distance from the transmitter's position to the kth point in the domain of interest.

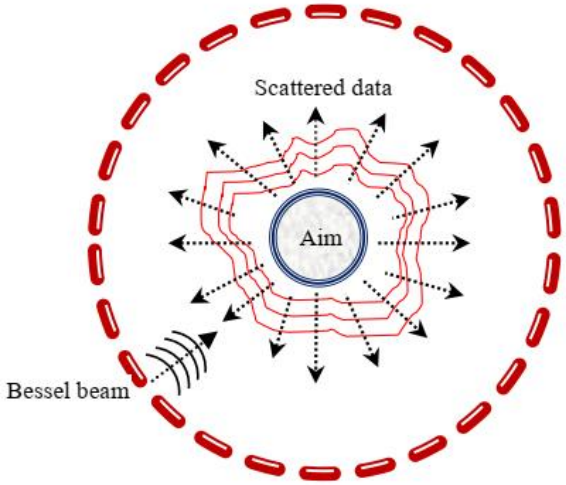


Figure 1. The studied DBIM's measurement configuration.

For a homogeneous medium, the signal received at the receiver is the incident wave. For example, in the presence of tumors, the medium becomes inhomogeneous. The following two situations may occur when the incident wave hits the target: (i) if the target size is much larger than the wavelength of the incident wave, it is reflected; (ii) if the target size is smaller than or equal to the wavelength of the incident wave, it is scattered in all directions around it. The Born iterative method is used to determine the linear relation between the scattered pressure difference and the sound contrast difference. The key to this method is that the scattering signal is considered very small compared to the incident signal, which is in line with the requirements to detect tumors in their early stages. Therefore, in this study, we address the reconstruction of targets with very small sound contrast, i.e., with very small scattering signals. In this case, the wave equation can be expressed as:

$$p\left(\vec{r}\right) = p^{inc}\left(\vec{r}\right) + p^{sc}\left(\vec{r}\right) \tag{2}$$

where $p^{sc}\left(\vec{r}\right)$, $p^{inc}\left(\vec{r}\right)$, and $p(\vec{r})$ are the scattered, incident, and total signals, respectively. It can be seen that the known data are the total signal and the incident signal. However, here, the concern is the reconstruction of the unknown $O(r)$ target from the obtained data, which is an inverse problem.

Consider that the wave numbers of the background and target mediums are k_0 and $k(r)$, respectively. Thus, according to [12], an inhomogeneous differential equation has the form:

$$\left(\nabla^2 + k_0^2(r)\right)p(r) = -O(r)p(r) \tag{3}$$

where $O(r)$ is the target function that needs to be calculated as:

$$O(r) = \begin{cases} k(r)^2 - k_0^2 = \omega^2\left(\frac{1}{c^2} - \frac{1}{c_0^2}\right) & if\ r \le R \\ 0 & if\ r > R \end{cases} \tag{4}$$

where c_0 and c are sound speeds in the background and target environments, respectively, ω is the incoming wave frequency, and R is the target's radius.

The Green function is an effective method to solve an inhomogeneous differential equation. Therefore, it is used to determine the nonlinear relationship between the scattered signal and the target based on the total and incident signals. Thus, Equation (2) can be rewritten using the Green function, $G_0(\cdot)$, as:

$$p\left(\vec{r}\right) = p^{inc}\left(\vec{r}\right) + \iint O\left(\vec{r}\right)p(\vec{r'})G_0\left(k_0, \left|\vec{r} - \vec{r'}\right|\right)d\vec{r'} \tag{5}$$

For the calculation of every pixel in the interested domain, the moment method (MoM) is used to estimate the pressure at points inside and outside the object of interest. The pressure in the grid points can be estimated by a vector of $N^2 \times 1$ size as:

$$\overline{p} = \left(\overline{I} - \overline{C}{\cdot}D\left(\overline{O}\right)\right)p^{inc} \tag{6}$$

and the exterior points offer a scattered vector of $N_tN_r \times 1$ size which is given as:

$$\overline{p}^{sc} = \overline{B}{\cdot}D\left(\overline{O}\right){\cdot}\ \overline{p} \tag{7}$$

where $\overline{B}$ is the matrix whose coefficients are Green functions, $G_0(r,r')$, from every pixel to the receiver's location, $\overline{C}$ is the matrix whose coefficients are Green functions, $G_0(r,r')$, among all pixels, $\overline{I}$ is an identity matrix, and $D(.)$ is a diagonalized operator.

Two variables ($\overline{p}$ and $\overline{O}$) are unresolved in Equations (6) and (7); to solve this, the first Born approximation is used, and these equations are rewritten as [20]:

$$\Delta p^{sc} = \overline{B}{\cdot}D(\overline{p}){\cdot}\Delta\overline{O} = \overline{M}{\cdot}\Delta\overline{O} \tag{8}$$

where $\overline{M} = \overline{B}{\cdot}D(\overline{p})$. With a transmitter and a receiver, a matrix ($\overline{M}$) and a scalar value (Δp^{sc}) are obtained. It can be noted that the unsolved $\overline{O}$ vector gives $N \times N$ variables that are equal to the pixel number in the domain of interest. $\Delta\overline{O}$ can be evaluated by solving the Tikhonov regularization problem [39]:

$$\Delta\overline{O} = \underset{\Delta\overline{O}}{\operatorname{argmin}}\|\Delta\overline{p}^{sc}{}_t - \overline{M_t}\Delta\overline{O}\|_2^2 + \gamma\|\Delta\overline{O}\|_2^2 \tag{9}$$

where $\Delta\overline{p}^{sc}$ is the $(N_tN_r \times 1)$ vector that carries the dissimilarity between the estimated and measured scattered data, $\overline{M}_t$ is the system $(N_tN_r \times N^2)$ matrix created by N_tN_r distinct $\overline{M}_t$ matrixes, and γ is the regularized parameter.

The DBIM process is described by Algorithm 1.

Algorithm 1. Distorted Born Iterative Method (DBIM)

Choose initial values: $\overline{O}_{(n)}$= $\overline{O}_{(0)}$ and $\overline{p}_0 = \overline{p}^{inc}$ using Equation (1)
For $n = 1$ *to* N_{DBIM}, **do**
1. Calculate $\overline{B}$ and $\overline{C}$
2. Calculate p, $\overline{p}^{sc}$ corresponding to $\overline{O}_{(n)}$ using Equations (6) and (7)
3. Calculate $\Delta\overline{p}^{sc}$ using Equation (8)
4. Calculate $\Delta\overline{O}_{(n)}$ using Equation (9)
5. Calculate $\overline{O}_{(n+1)} = \overline{O}_{(n)} + \Delta\overline{O}_{(n)}$
End For

To quantify the efficiency of the proposed approach, target functions were acquired in order to obtain the experimental data to be used in the iterative reconstruction of the target image. Then, the error in the reconstructed image was determined and compared to the original image at each iteration. Thus, by supposing that m is a $P \times Q$ original image, i.e., the ideal target function, and $\hat{m}$ is the reconstructed image, the normalized absolute error (RRE) could be defined as:

$$RRE = \frac{1}{PxQ} \sum_{i=1}^{P} \sum_{j=1}^{Q} \frac{|m_{ij} - \hat{m}_{ij}|}{|m_{ij}|} \tag{10}$$

3. Results

3.1. Multi-Resolution DBIM Approach

For the multi-resolution DBIM approach, the nearest neighbor interpolation was used; this is one of the simplest ways to double the image size, by replacing each pixel with four pixels of the same color. Using this interpolation technique, the obtained result is larger than the original image, while preserving all the details of the original image. There are many different types of complex interpolation algorithms, such as bilinear, bicubic, and spline-based, but the nearest neighbor technique was selected because of its advantages of consuming little computational time and not generating new data values [40].

The implementation process of the one-step multi-resolution DBIM (one-step MR-DBIM) was:

$$N_{11} \times N_{11} \rightarrow N_{22} \times N_{22}$$

The number of iterations implemented with a raw mesh integrated area of $N_{11} \times N_{11}$ size is denoted as N_{N11}, so the number of iterations implemented with one of $N_{22} \times N_{22}$ size is $N_{\mathrm{N22}} = N_{sum} - N_{N11}$.

The implementation process of the multi-resolution DBIM: four-step MR-DBIM, was:

$$N_1 \times N_1 \rightarrow \mathrm{N}_2 \times N_2 \rightarrow N_3 \times N_3 \rightarrow N_4 \times N_4$$

The number of implemented iterations with the mesh integrated area of $N_1 \times N_1$, $N_2 \times N_2$, $N_3 \times N_3$, and $N_4 \times N_4$ sizes are denoted as N_{N1}, N_{N2}, N_{N3}, and N_{N4}, respectively.

Here, the simulation parameters used were: frequency, f = 0.64 MHz, N_t = 11, N_r = 22, N_{sum} = 8, N_{N11} = 17, N_{N22} = 33, N_1 = 5, N_2 = 9, N_3 = 17, N_4 = 33, N_{N1} = 1, N_{N2} = 1, N_{N3} = 1, N_{N4} = 5, the scattering area diameter was 7.3 mm, the sound contrast was 30%, the Gaussian noise was 10%, the speed of sound in the background was equal to 1540 m/s, and the distances from the transmitters and receivers to the center of the object were equal to 50 and 60 mm, respectively.

The computational cost for the imaging system is: $O\left(N_{\mathrm{iter}} N_t N_r N^2\right)$, where N_{iter} is the number of iterations, N_t is the number of transmitters, N_r is the number of receivers, and N is the number of pixels, respectively. The numerical simulation was performed using MATLAB running on a PC with an Intel core i3 processor and 2 GB of RAM.

As a result of its well-known properties, the Bessel function [38] is usually used in numerical simulations as a transmitted signal, which is termed an incident wave, whose

frequency is f; therefore, it is a monochromatic wave. The wavelength (λ) of this wave is calculated as $\lambda = c_0/f$, where c_0 is the sound speed in the background medium. The frequency of the incident signal was selected based on previous work [24] as equal to 0.64 MHz. The propagation speed of ultrasound waves in the women's breast environment is in the range of 1350 to 1600 m/s, and in the background medium, it is approximately 1484 m/s [41]. That is, the difference in the propagation speed in women's breasts ranges from 0 to 15.6%. However, in this study, a more demanding problem was addressed, i.e., a strong scattering medium was investigated; thus, a sound contrast of 30% was taken into account.

In DBIM, the specific value of each pixel is calculated in the region of interest. As long as there is a heterogeneous medium of a small size equivalent to the incident wavelength, the ultrasonic wave will be scattered, and scattering data are obtained. Using DBIM, the exact position and shape of the object can be determined. Thus, one can see that the core problem is the algorithm's ability to accurately recover the object with high performance. Accordingly, here, in the process of designing the DBIM simulation scenario, the adopted model and parameters were defined based on the purpose of developing a better image recovery algorithm than the traditional one. Therefore, a simple circular cylinder was selected as the object to be restored, and the environment around it was defined as uniform. Then, the focus of the investigation became how to recover the image as close as possible to the objective function. Thus, the parameter used to restore the ideal object was the sound contrast, and the density and attenuation parameters were not considered. A study regarding the effect of the acoustic density, attenuation, and compressibility profile parameters on the obtained images can be found in [42].

Figure 2 shows the ideal functions, i.e., the ground truth, of the objects to be imaged. The larger the number of involved pixels, the larger the number of variables to find and recover, and thus, the imaging system becomes more complex.

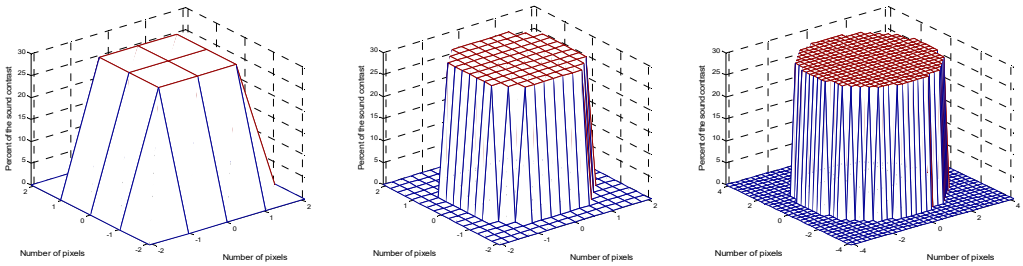


Figure 2. Ideal functions of the objects of interest in terms of the number of involved pixels: 5 (**a**), 17 (**b**), and 33 (**c**), respectively.

The smallest value of N_1 was investigated for the first raw meshed integration area, which offers the best performance, leading to Table 1. It is clear from the data in Table 1 that the value of N_1 equal to 5 led to the best performance. Therefore, N_1 = 5 was chosen for a deeper simulation.

Figure 3 presents the error performance of the four-step MR-DBIM proposed method relative to the other methods under comparison. It can be observed that the normalized error was decreased in comparison with the DBIM and one-step MR-DBIM methods. With the one-step MR-DBIM method, it can be reasoned that the RRE decreased over each iteration because for the same number of measurements, estimating the smaller ($N_{11} \times N_{11}$) object with N_{N11} = 17 was better than immediately estimating the large ($N_{22} \times N_{22}$) object with the DBIM's N_{N22} = 33. Therefore, a good estimate from the initial loop leads to a better estimate of this one-step MR-DBIM method. As for the four-step MR-DBIM method, one can see that there was a maximum point at the fourth loop, which is understandable because, in the fourth loop, the object with the largest ($N_4 \times N_4$) size (desired value) was restored. With the same number of measurements, the largest number of pixels is the

largest number of variables, so the estimation will be the most difficult; hence the RRE will be the largest. In loops one and two, the RRE was quite small due to the small number of variables, so the estimation was quite good in these loops.

Table 1. Error after the first iteration using $N_1 \times N_1$ (NoC-no convergence, best value in bold).

N_1	1	2	3	4	5
Error	NoC	NoC	0.1572	0.1280	**0.1229**
N_1	6	7	8	9	10
Error	0.2082	0.4898	0.5078	0.5278	0.4525
N_1	11	12	13	14	15
Error	0.5725	0.6408	0.6957	0.6304	0.6256
N_1	16	17	18	19	20
Error	0.5991	0.6302	0.5991	0.6215	0.6288

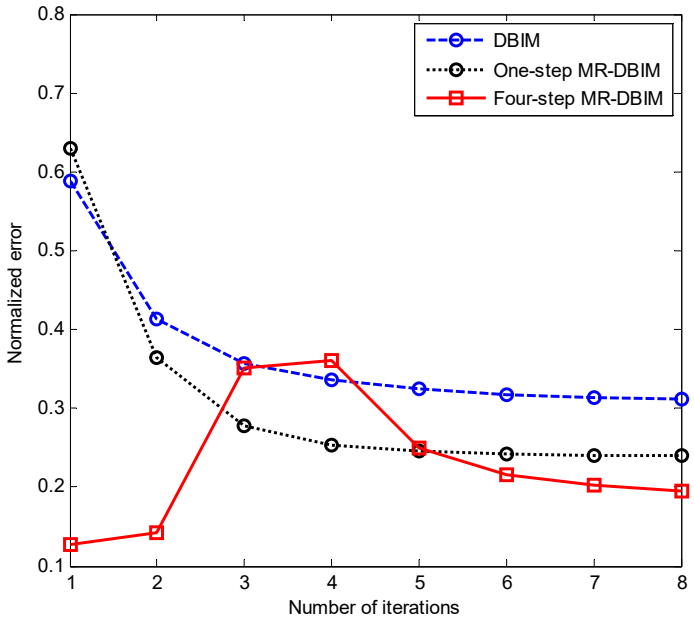


Figure 3. Normalized error comparison among the DBIM, one-step MR-DBIM, and four-step MR-DBIM methods.

The total runtime required by the DBIM, one-step MR-DBIM, and four-step MR-DBIM methods after N_{sum} iterations was calculated. It was found that the imaging time with the DBIM method was the largest, which was equal to 640.7 s; then, as the interpolation level increased, the imaging time decreased, leading to 569.8 s for the one-step interpolation, and 405.5 s for the four-step interpolation. This finding makes sense since, in DBIM, the number of variables, or pixels, ($N_4 \times N_4$) does not change in each loop. However, with the interpolation, the number of pixels gradually increases until $N_4 \times N_4$, so the number of variables in the previous loops will be significantly less than in the DBIM method; therefore, the imaging time will be significantly reduced.

Figure 4 shows the reconstructed results of the DBIM, one-step MR-DBIM, and four-step MR-DBIM methods through the iterations. Through visual observation, one can realize that, in the DBIM method, there was not much difference between the recovery results through the loops. However, there was a clear difference in the recovered image in the four-step MR-DBIM method, especially in loops one to four. This is because, in these loops, the number of pixels was small, i.e., a small number of variables, so the estimation was quite accurate for these loops. It is critical to accurately assess the object in the first iteration

so that one can more accurately estimate during later iterations. This dramatically reduces noise in the restored image, especially in the first loops.

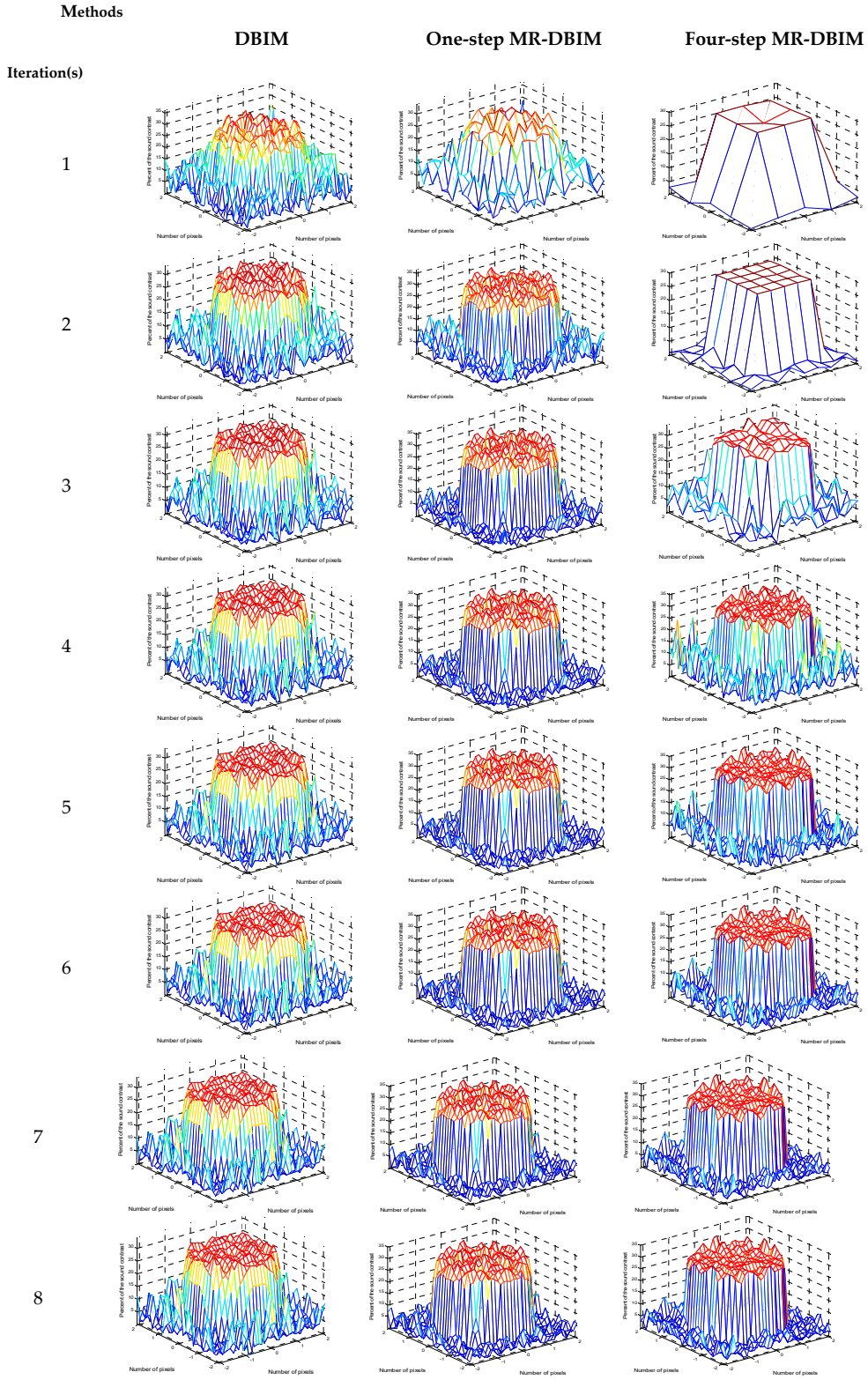


Figure 4. Reconstructed results of the DBIM, one-step MR-DBIM, and four-step MR-DBIM methods through the iterations (horizontal axes represent the lambda wavelength, and vertical axes represent the sound contrast).

3.2. Multi-Resolution and Multi-Frequency DBIM Approach

Obviously, the multi-resolution and multi-frequency DBIM approach (MR-MF-DBIM) can reduce the image formation time and, especially, can estimate the object of interest quite accurately in the first iterations. Therefore, for the proposed method, in the first loops, mainly in the first four loops, a small frequency of 0.64 MHz was used to satisfy the Born approximation condition. Then, starting at the fifth loop, when the number of pixels, i.e., the number of variables, reaches the desired value as a maximum, the frequency was adjusted incrementally to overcome the noise effectively, and the increased frequency also increased the resolution of the recovered image.

The simulation parameters used in the this experiment for the proposed MR-MF-DBIM method were: frequency, f = 0.64 MHz, $f_1 = 2f$, $f_2 = 3f$, $f_3 = 4f$, $f_4 = 5f$, N_t = 11, N_r = 22, N_{sum} = 8, N_1 = 5, N_2 = 9, N_3 = 17, N_4 = 33, N_{N1} = 1, N_{N2} = 1, N_{N3} = 1, N_{N4} = 5, N_{N4f} = 1, N_{N4f1} = 1, N_{N4f2} = 1, N_{N4f3} = 1, N_{N4f4} = 1, scattering area diameter = 7.3 mm, sound contrast of 30%, Gaussian noise of 10%, and distances from transmitters and receivers to the center of the object of interest of 50 and 60 mm, respectively.

Figure 5 presents the error performance of the proposed MR-MF-DBIM method relative to the MR-DBIM method. The normalized error was decreased in comparison with the four-step MR-DBIM method. It can also be seen that starting from the fourth loop onwards, the RRE reduced accordingly as the frequency increased. This occurs because the frequency increase can effectively correct the noise, and the estimation is better due to the gradual updating of the image's sound contrast.

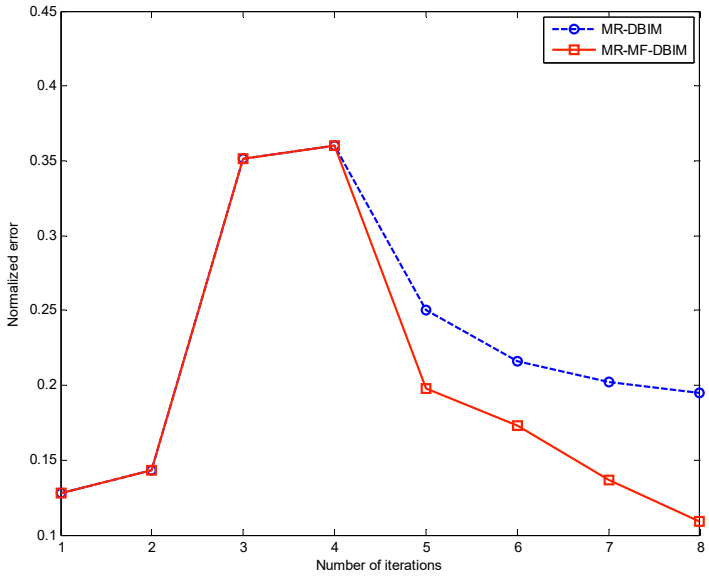


Figure 5. Normalized error comparison between the MR-MF-DBIM and four-step MR-DBIM methods.

The total runtimes of the MR-MF-DBIM and four-step MR-DBIM methods after N_{sum} iterations were calculated. Although the RRE of the MR-MF-DBIM method was significantly reduced relative to the four-step MR-DBIM method, the imaging time was increased by just 8.9%. This occurred because in the MR-MF-DBIM method, mainly in loops five to eight, the frequency increases, and the numerical value of the imaging matrix is also significant, which makes the computation longer.

Figure 6 shows the reconstructed results of the MR-MF-DBIM and four-step MR-DBIM methods through the iterations. In the first four iterations, the recovered images of both methods were exactly the same because there is no difference in the algorithms. However, starting from loop five, due to the use of the MF technique in the MR-MF-DBIM method, it is intuitively obvious that the noise, especially the background noise, was significantly reduced, which led to a better image estimation.

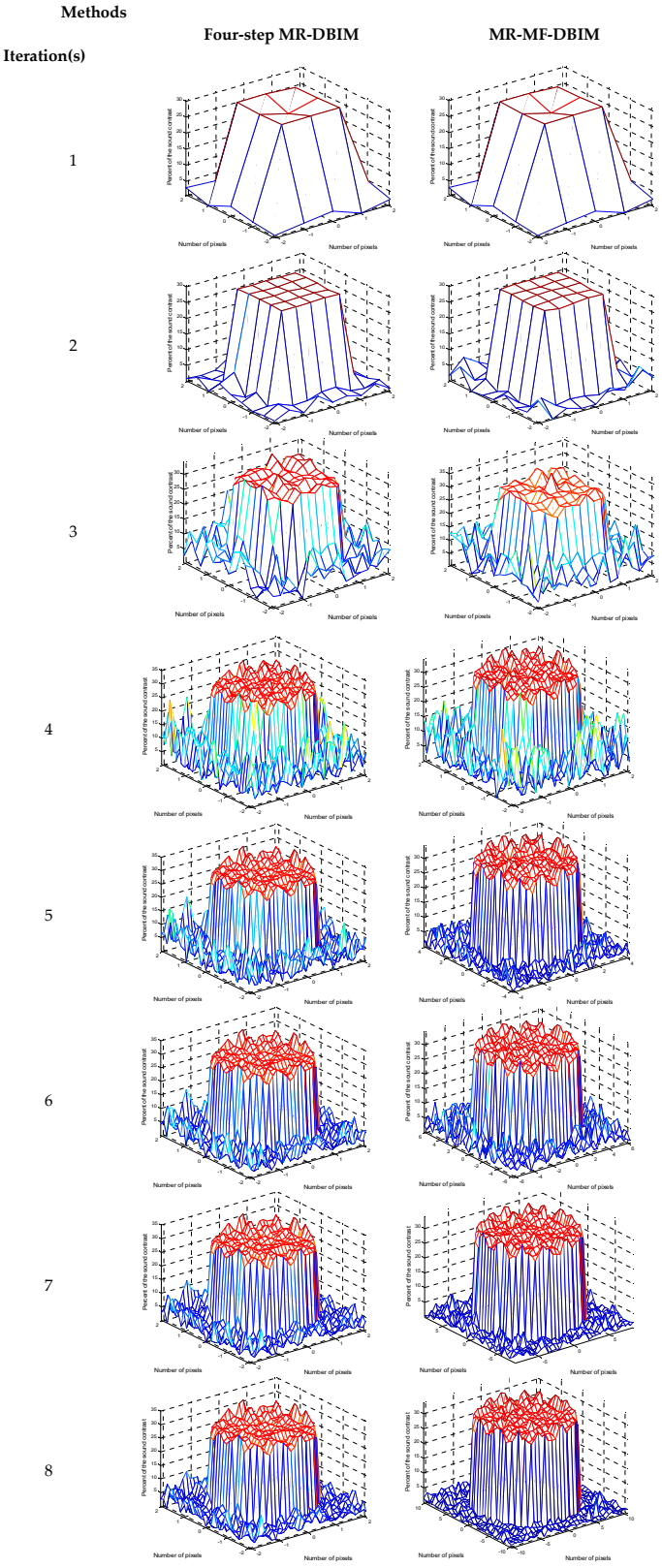


Figure 6. Reconstructed results of the MR-MF-DBIM and four-step MR-DBIM methods through the iterations (horizontal axes represent the lambda wavelength, and vertical axes represent the sound contrast).

With the MR-DBIM method, the imaging quality can be improved (Figure 3), and the imaging process can be accelerated. However, a multi-frequency technique was used

to reduce the noise and reconstruct images of higher resolution to meet the actual application requirements. Indeed, with the MR-MF-DBIM method, the background noise in the recovered target was decreased relative to the MR-DBIM method (Figure 6). Thus, the multi-frequency technique can produce images with a higher resolution as suggested in [27,28].

It could be realized that the more data collected, the more accurate the reconstruction. The number of measurements in the DBIM depends on the product of the number of transmitters and receivers. In Figure 7, one can observe the quality of the reconstructed image in terms of the number of measurements used during the proposed MR-MF-DBIM method, mainly according to the following five scenarios, $N_t \times N_r$ equal to: $11 \times 22 = 242$, $13 \times 24 = 312$, $15 \times 26 = 390$, $17 \times 28 = 476$, and $19 \times 30 = 570$ measurements. It could be observed that, as the number of measurements increased, the normalized error decreased, which indicates an increase in the imaging quality. This makes sense because, since the number of variables, i.e., the number of pixels, remains constant as the number of measurements increases, more data can be collected, and thus the object of interest can be more accurately reconstructed.

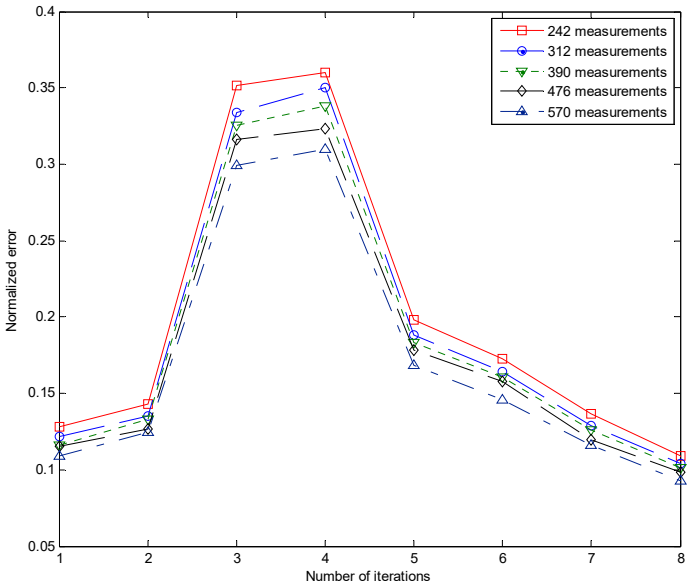


Figure 7. Effect of the number of measurements on the quality of the reconstructed image.

Figure 8 allows us to analyze the quality of the reconstructed image using MR-MF-DBIM in terms of the sound contrast between the object and background environment. It was found that, as the sound contrast increases, the imaging quality decreases. This can be explained by the limitation of the Born approximation. Hence, the main limitation of DBIM is that divergence occurs when $\Delta\varphi > \pi$, where $\Delta\varphi = 2\omega\left(\frac{1}{c} - \frac{1}{c_0}\right)R$ [43]. Therefore, the incident frequency (f) must be $< \frac{c_0}{2d \times \%\Delta c}$. In the case of the wave propagation speed in the background medium (c_0) being equal to 1540 m/s and the object diameter being 7.3 mm, which corresponds to sound contrasts of 10, 15, 20, 25, and 30%, f must be <1.05, 0.70, 0.53, 0.42, and 0.35 MHz, respectively. Therefore, with the transmitter's frequency in the simulation set equal to 0.64 MHz, the Born approximation condition was satisfied with sound contrasts of 10 and 15%. In these cases, the quality of the reconstructed image was quite good and a small normalized error was obtained. On the other hand, when the Born condition was not respected, mainly with sound contrasts of 20, 25, and 30%, it was observed that the normalized error increased. However, here, a more demanding problem was also addressed: image reconstruction under a high contrast of 30%. Although the condition of the Born approximation method was not respected, the object of interest was still successfully reconstructed, despite having been affected by artifacts near its center.

Thus, a good solution from the Born approximation method was still achieved. This was also investigated in [12].

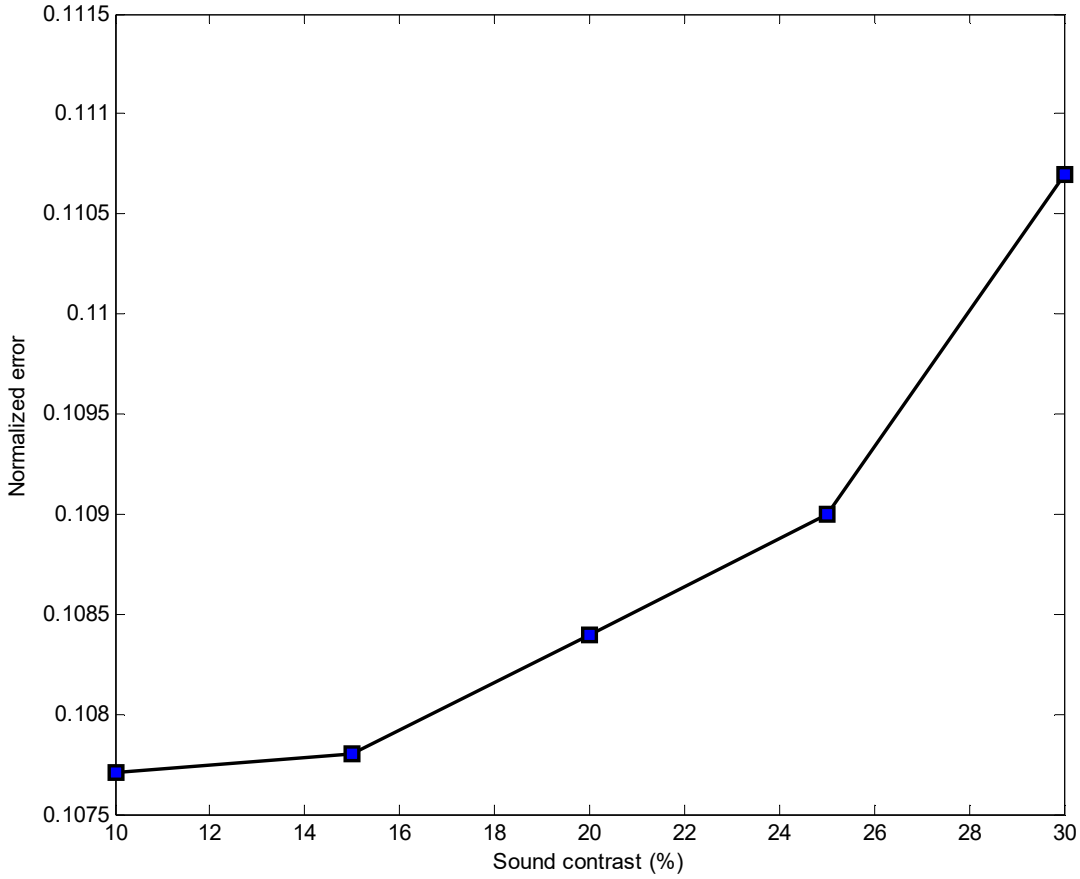


Figure 8. Quality of the reconstructed image using MR-MF-DBIM in terms of the sound contrast between the object and background environment.

Figures 9 and 10 show the reconstructions obtained using the MR-DBIM (Figures 9a and 10a) and MR-MF-DBIM (Figures 9b and 10b) methods after the eighth iteration in the cases of two and three cylinders in the region of interest, respectively. The RREs obtained for MR-DBIM and MR-MF-DBIM methods were equal to 0.3828 and 0.2880 for the case of two cylinders, and 0.4577 and 0.3579 for the case of three cylinders, respectively. Compared with the MR-DBIM method, the RRE of MR-MF-DBIM decreased by 24.76% in the case of two cylinders and 21.80% in the case of three cylinders. Visually, one can observe that the noise in the background and objects is significantly reduced, especially in the case of two cylinders. This can be explained by the effect of gradually increasing the frequency, which can reduce noise and improve the resolution of the recovered image. Indeed, at the lower frequency, the original image is recovered with a contrast of c_1. Then, at a higher frequency, the image is recovered with a contrast of c_2 that is higher than c_1. In fact, simply by continuously increasing the frequency, it is possible to gradually achieve the desired level of contrast in the object of interest, i.e., c_*, with $c_1 < c_2 < \ldots < c_*$. The importance of such a gradual increase in frequency is that it gradually increases the resolution of the recovered image, which could possibly lead to image restoration at the biological tissue level.

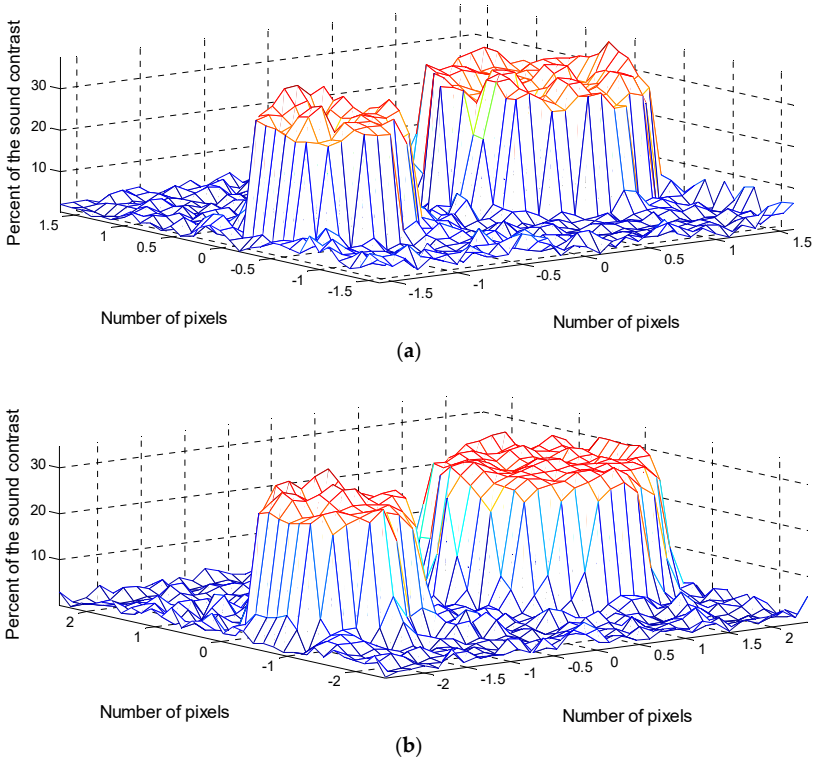


Figure 9. Reconstructions obtained for the two-cylinders case after the eighth iteration using (**a**) MR-DBIM and (**b**) MR-MF-DBIM.

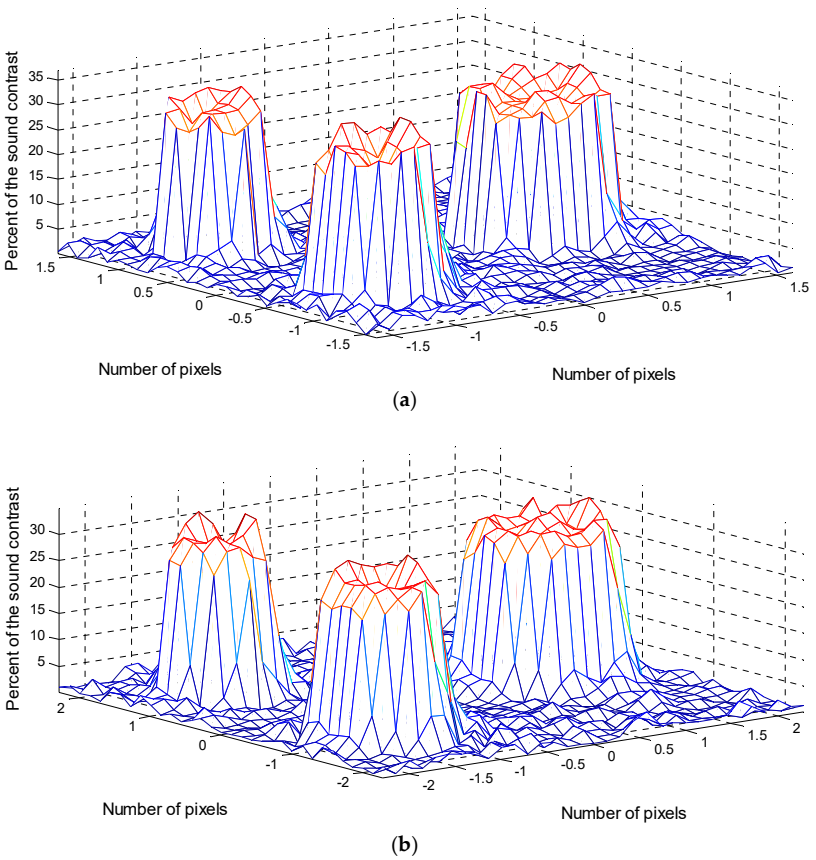


Figure 10. Reconstructions obtained for the three-cylinders case after the eighth iteration using (**a**) MR-DBIM and (**b**) MR-MF-DBIM.

4. Conclusions

The distorted Born iterative method, a quantitative method with great potential in reconstructing a target at a comparable size by the incident wavelength, has been used for imaging an object of interest in a strong scattering medium. This article presents the multi-resolution technique, which is a four-step interpolation scheme, applied to the DBIM method to speed up and enhance the imaging quality of the object of interest.

The imaging results revealed that the RRE was reduced by 18.67 and 37.21% relative to the multi-resolution technique (one-step interpolation) and DBIM methods, respectively. Furthermore, the integration of the multi-resolution and multi-frequency techniques was also considered for high-contrast object imaging, and the reduced normalized absolute error was reduced by 44.01% relative to the MR-DBIM method.

The proposed method holds promise for imaging objects at the biological tissue level, and experiments using real data should be performed in order to confirm this. Furthermore, this method could be extended to 3D imaging in future research.

Author Contributions: Conceptualization, T.Q.-H. and T.D.-T.; methodology, L.T.T., T.Q.-H. and T.D.-T.; software, L.T.T.; validation, T.D.-N., V.K.S. and J.M.R.S.T.; formal analysis, L.T.T.; investigation, T.D.-N.; resources, T.D.-T.; data curation, T.D.-N.; writing-original draft preparation, L.T.T. and T.Q.-H.; writing-review and editing, T.D.-T., V.K.S. and J.M.R.S.T.; visualization, T.Q.-H.; supervision, T.D.-T., V.K.S. and J.M.R.S.T.; project administration, V.K.S.; funding acquisition, J.M.R.S.T. All authors have read and agreed to the published version of the manuscript.

Funding: This work was supported by National Foundation for Science and Technology Development (NAFOSTED) under Grant 103.05-2020.13.

Institutional Review Board Statement: Not applicable.

Informed Consent Statement: Not applicable.

Data Availability Statement: Not applicable.

Conflicts of Interest: The authors declare no conflict of interest.

References

1. Schueler, C.F.; Lee, H.; Wade, G. Fundamentals of digital ultrasonic processing. *IEEE Trans. Sonics Ultrason.* **1984**, *31*, 195–217. [CrossRef]
2. Macovski, A. Ultrasonic imaging using arrays. *Proc. IEEE* **1979**, *67*, 484–495. [CrossRef]
3. Kino, G.S. Acoustic Waves: Devices, Imaging, and Analog Signal Processing. In *Englewood Cliffs*; Prentice Hall: Hoboken, NJ, USA, 1987.
4. Zhu, Q.; Steinberg, B.D. Wavefront amplitude distortion and image sidelobe levels: Part I—Theory and computer simulations. *IEEE Trans. Ultrason. Ferroelectr. Freq. Control* **1993**, *40*, 747–753. [CrossRef] [PubMed]
5. Greenleaf, J.; Johnson, S.; Samayoa, W.; Duck, F. Algebraic reconstruction of spatial distributions of acoustic velocities in tissue from their time-of-flight profiles. *Acoust. Hologr.* **1975**, *6*, 71–90.
6. Greenleaf, J.; Johnson, S.; Lee, S.; Herman, G.; Wood, E. Algebraic reconstruction of spatial distributions of acoustic absorption within tissue from their two-dimensional acoustic projections. *Acoust. Hologr.* **1974**, *5*, 591–603.
7. Johnson, S.A.; Greenleaf, J.F.; Samayoa, W.A.; Duck, F.A.; Sjostrand, J. Reconstruction of three-dimensional velocity fields and other parameters by acoustic ray tracing. In Proceedings of the IEEE Ultrasonics Symposium, Los Angeles, CA, USA, 22–24 September 1975; pp. 46–51.
8. Duric, N.; Littrup, P.; Babkin, A.; Chambers, D.; Azevedo, S.; Kalinin, A.; Pevzner, R.; Tokarev, M.; Holsapple, E.; Rama, O.; et al. Development of ultrasound tomography for breast imaging: Technical assessment. *Med. Phys.* **2005**, *32*, 1375–1386. [CrossRef] [PubMed]
9. Li, C.; Duric, N.; Huang, L. Breast imaging using transmission ultrasound: Reconstructing tissue parameters of sound speed and attenuation. In Proceedings of the International Conference on BioMedical Engineering and Informatics, Sanya, China, 27–30 May 2008; Volume 2, pp. 708–712.
10. Jeong, J.-W.; Kim, T.-S.; Shin, D.C.; Do, S.; Singh, M.; Marmarelis, V.Z. Soft tissue differentiation using multiband signatures of high resolution ultrasonic transmission tomography. *IEEE Trans. Med. Imaging* **2005**, *24*, 399–408. [CrossRef]
11. Johnson, S.A.; Abbott, T.; Bell, R.; Berggren, M.; Borup, D.; Robinson, D.; Wiskin, J.; Olsen, S.; Hanover, B. Noninvasive breast tissue characterization using ultrasound speed and attenuation. *Acoust. Imaging* **2007**, *28*, 147–154.
12. Kak, A.; Slaney, M. Principles of Computerized Tomographic Imaging. In *Philadelphia*; SIAM: University City, PA, USA, 2001.

13. Greenleaf, J.; Ylitalo, J.; Gisvold, J. Ultrasonic computed tomography for breast examination. *IEEE Eng. Med. Biol. Mag.* **1987**, *6*, 27–32. [CrossRef] [PubMed]
14. Andre, M.P.; Janee, H.S.; Martin, P.J.; Otto, G.P.; Spivey, B.A.; Palmer, D.A. High-speed data acquisition in a diffraction tomography system employing large-scale toroidal arrays. *Int. J. Imaging Syst. Technol.* **1997**, *8*, 137–147. [CrossRef]
15. Wiskin, J.; Borup, D.; Johnson, S.; Berggren, M.; Abbott, T.; Hanover, R. Full wave, nonlinear, inverse scattering. *Acoust. Imaging* **2007**, *28*, 183–194.
16. Lasaygues, P.; Franceschini, E.; Guillermin, R.; Lefebvre, J.-P.; Salaud, N.; Petit, P. Two-dimensional ultrasonic computed tomography of growing bones. In Proceedings of the IEEE Ultrasonics Symposium, New York, NY, USA, 28–31 October 2007; Volume 1, pp. 1816–1819.
17. Devaney, A. Inversion formula for inverse scattering within the Born approximation. *Opt. Lett.* **1982**, *7*, 111–112. [CrossRef] [PubMed]
18. Devaney, A. Inverse-scattering theory within the Rytov approximation. *Opt. Lett.* **1981**, *6*, 374–376. [CrossRef]
19. Chew, W.C.; Wang, Y.M. Reconstruction of two-dimensional permittivity distribution using the distorted Born iterative method. *IEEE Trans. Med. Imaging* **1990**, *9*, 218–225. [CrossRef]
20. Haddadin, O.S.; Ebbini, E.S. Solution to the inverse scattering problem using a modified distorted Born iterative algorithm. In Proceedings of the IEEE Ultrasonics Symposium, Seattle, WA, USA, 7–10 November 1995; pp. 1411–1414.
21. Gang, Y.; Lim, K.H.; George, R.; Ybarra, G.; Joines, W.T.; Liu, Q.H. A 3D EIT system for breast cancer imaging. In Proceedings of the 3rd IEEE International Symposium on Biomedical Imaging: Nano to Macro, Arlington, VA, USA, 6–9 April 2006; pp. 1092–1095.
22. Abdi, M.; Liatsis, P. EIT in Breast Cancer Imaging: Application to Patient-Specific Forward Model. In Proceedings of the 2011 Developments in E-systems Engineering, Dubai, United Arab Emirates, 6–8 December 2011; pp. 56–61.
23. Quang-Huy, T.; Nguyen, K.T.; Doan, P.T.; Tran, D. Interpolated Hybrid DBIM Approach for Enhanced Imaging in Ultrasound Tomography. *Res. Biomed. Eng. (RBME)* **2022**, *38*, 389–400. [CrossRef]
24. Theu, L.T.; Tran, Q.; Solanki, V.K.; Shemeleva, T.R.; Tran, D. Influence of the multi-resolution technique on tomographic reconstruction in ultrasound tomography. *Int. J. Parallel Emergent Distrib. Syst.* **2021**, *36*, 579–593. [CrossRef]
25. Quang-Huy, T.; Nguyen, T.; Solanki, V.K.; Tran, D. An Enhanced Multi-Frequency Distorted Born Iterative Method for Ultrasound Tomography Based on Fundamental Tone and Overtones. *Int. J. Inf. Retr. Res. (IJIRR)* **2022**, *12*, 1–19. [CrossRef]
26. Haddadin, O.S.; Ebbini, E.S. Multiple frequency distorted Born iterative method for tomographic imaging. In *Acoustical Imaging*; Springer: Boston, MA, USA, 1997; pp. 613–619.
27. Haddadin, O.S.; Ebbini, E.S. Imaging strongly scattering media using a multiple frequency distorted Born iterative method. *IEEE Trans. Ultrason. Ferroelectr. Freq. Control* **1998**, *45*, 1485–1496. [CrossRef]
28. Tijhuis, A.G.; Belkebir, K.; Litman, A.C.; de Hon, B.P. Multiple-frequency distorted-wave Born approach to 2D inverse profiling. *Inverse Probl.* **2001**, *17*, 1635. [CrossRef]
29. Lavarello, R.; Oelze, M. Density imaging using a multiple-frequency DBIM approach. *IEEE Trans. Ultrason. Ferroelectr. Freq. Control* **2010**, *57*, 2471–2479. [CrossRef] [PubMed]
30. Tran, Q.H.; Tran, D.T.; Huynh, H.T.; Ton-That, L.; Nguyen, L.T. Influence of dual-frequency combination on the quality improvement of ultrasound tomography. *Simulation* **2016**, *92*, 267–276. [CrossRef]
31. Varray, F.; Cachard, C.; Kybic, J.; Novell, A.; Bouakaz, A.; Basset, O. A multi-frequency approach to increase the native resolution of ultrasound images. In Proceedings of the 20th European Signal Processing Conference (EUSIPCO), Bucharest, Romania, 27–31 August 2012; pp. 2733–2737.
32. Sayed, I.S. Multi-frequency ultrasound imaging: Phantom study. *Int. J. Allied Health Sci.* **2018**, *2*, 304–309.
33. Miao, Z. Implementation and Optimisation of Microwave Medical Imaging Based on the Multiple-Frequency Dbim-Twist Algorithm. Ph.D. Thesis, King's College London, London, UK, 2018.
34. Ahsan, S.; Guo, Z.; Miao, Z.; Sotiriou, I.; Koutsoupidou, M.; Kallos, E.; Kosmas, P. Design and experimental validation of a multiple-frequency microwave tomography system employing the DBIM-TwIST algorithm. *Sensors* **2018**, *18*, 3491. [CrossRef]
35. Miao, Z.; Kosmas, P. Multiple-frequency DBIM-TwIST algorithm for microwave breast imaging. *IEEE Trans. Antennas Propag.* **2017**, *65*, 2507–2516. [CrossRef]
36. Lu, P.; Corcoles, J.; Kosmas, P. Enhanced FEM-based DBIM approach for two-dimensional microwave imaging. *IEEE Trans. Antennas Propag.* **2020**, *69*, 5187–5192. [CrossRef]
37. Saraskanroud, F.M.; Jeffrey, I. Hybrid Approaches in Microwave Imaging using Quantitative Time-and Frequency-Domain Algorithms. *IEEE Trans. Comput. Imaging* **2022**, *8*, 121–132. [CrossRef]
38. Krainov, V.P.; Reiss, R.H.; Smirnov, M.B. Appendix J: Properties of the Generalized Bessel Function. In *Radiative Processes in Atomic Physics*; John Wiley & Sons: New York, NY, USA, 2005.
39. Golub, G.H.; Hansen, P.C.; O'Leary, D.P. Tikhonov Regularization and Total Least Squares. *SIAM J. Matrix Anal. Appl.* **1999**, *21*, 185–194. [CrossRef]
40. Jegou, H.; Douze, M.; Schmid, C. Product quantization for nearest neighbor search. *IEEE Trans. Pattern Anal. Mach. Intell.* **2011**, *33*, 117–128. [CrossRef]
41. Greenleaf, J.F.; Bahn, R.C. Clinical imaging transmissive ultrasonic computerized tomography. *IEEE Trans. Biomed. Eng.* **1981**, *28*, 177–185. [CrossRef] [PubMed]

42. Mojabi, P.; LoVetri, J. Ultrasound tomography for simultaneous reconstruction of acoustic density, attenuation, and compressibility profiles. *J. Acoust. Soc. Am.* **2015**, *134*, 1813–1825. [CrossRef] [PubMed]
43. Slaney, M.; Kak, A.C.; Larson, L.E. Limitations of imaging with first order diffraction tomography. *IEEE Trans. Microw. Theory Tech.* **1984**, *32*, 860–873. [CrossRef]